Influence of shower fluctuations and primary composition on studies of the shower longitudinal development

Jaime Alvarez-Muñiz,* Ralph Engel,† T.K. Gaisser, Jeferson A. Ortiz,‡ and Todor Stanev
Bartol Research Institute,
University of Delaware, Newark, Delaware 19716, U.S.A.

We study the influence of shower fluctuations, and the possible presence of different nuclear species in the primary cosmic ray spectrum, on the experimental determination of both shower energy and the proton air inelastic cross section from studies of the longitudinal development of atmospheric showers in fluorescence experiments. We investigate the potential of track length integral and shower size at maximum as estimators of shower energy. We find that at very high energy ($\sim 10^{19} - 10^{20}$ eV) the error of the total energy assignment is dominated by the dependence on the hadronic interaction model, and is of the order of 5%. At lower energy ($\sim 10^{17} - 10^{18}$ eV), the uncertainty of the energy determination due to the limited knowledge of the primary cosmic ray composition is more important. The distribution of shower maximum, $X_{\rm max}$, is discussed as a measure of the proton-air cross section. Uncertainties in a possible experimental measurement of this cross section introduced by intrinsic shower fluctuations, the model of hadronic interactions, and the unknown mixture of primary nuclei in the cosmic radiation are numerically evaluated.

PACS numbers: 96.40.Pq,96.40.-z,13.85.-t

I. INTRODUCTION

The fluorescence technique of ultra high energy cosmic ray (UHECR) detection was first explored in the pioneering Fly's Eye detector [1], and is currently being used in its successor, the high resolution Fly's Eye (HiRes) [2], as well as in the Pierre Auger Observatory [3] that is currently under construction. The underlying idea is the detection of atmospheric nitrogen fluorescence light induced by the passage of charged particles through the atmosphere. The number of charged particles at depth X in the atmosphere, $N(X)$, i.e. the longitudinal shower profile, can be extracted from data because $N(X)$ is to a good approximation proportional to the amount of emitted fluorescence light. In this approximation, the total energy that goes into electrons and positrons (the electromagnetic energy $E_{\rm em}$ from now on) is obtained by integration of the shower longitudinal profile [4]

$$E_{\rm em} = \alpha_{\rm eff} \int_0^\infty N(X) dX \qquad (1)$$

where $\alpha_{\rm eff}$ is the average (effective) ionization loss rate which is usually taken as a constant over the entire shower and is given by ~ 2.19 MeV/g cm^{-2} [4, 5].

The integral on the right hand side of Eq. (1) represents the total track length of all charged particles in the shower projected onto the shower axis. Electrons and positrons constitute the bulk of the charged particles in a shower and contribute most to the production of fluorescence light. In the following we neglect the contribution of muons and other charged particles to the production of fluorescence light, which is of the order of 2% (see discussion in [6]).

It is generally assumed that the fluorescence rate is proportional to the ionization energy loss rate dE/dX, although this has been experimentally proved only to some extent [7, 8]. Consequently in order to estimate shower energy, there is in principle no need to convert the measured fluorescence intensity first to a particle number, and then relate the total track length to the energy of the shower through Eq. (1). The total ionization energy deposit can instead be obtained from the fluorescence intensity and can be used directly as an energy estimate [9]. However, as long as the lateral spread of shower particles is correctly accounted for [10], the conversion of fluorescence light intensity to number of particles and then to energy through Eq. (1) does not lead in principle to observable errors mainly for two reasons: Firstly the ionization energy deposit depends only weakly on the particle energy, and secondly the shape of the energy spectrum of particles in an air shower changes only slowly with the traversed depth. Only in the very early evolution stage of a shower is the particle energy spectrum significantly harder than that at the shower maximum. The corresponding energy deposit is higher by up to a factor of 1.5, but due to the small number of particles, the resulting error in the energy estimation is negligible [11].

There are several additional factors, such as air pressure, density and humidity, that influence the relation of the fluorescence intensity to energy deposit and particle numbers. The discussion of these aspects, including the conversion of the observed light curve to a longitudinal

*Electronic address: jaime@fpaxp1.usc.es; Now at Dept. de Física de Partículas, Facultade de Física, Universidade de Santiago de Compostela, 15706 Santiago de Compostela, A Coruña, Spain
†Now at Forschungszentrum Karlsruhe, Institut für Kernphysik, Postfach 3640, 76021 Karlsruhe, Germany
‡Now at Instituto de Astronomia, Geofísica e Ciências Atmosféricas, Universidade de São Paulo, Caixa Postal 3386, São Paulo, SP 01060-970, Brasil

shower profile are beyond the scope of this work.

In this article we investigate the longitudinal shower profile as an experiment-independent quantity and study its relation to the energy and mass of the primary particle. In Sec. II the track length integral and the particle number at shower maximum are compared as energy estimators under the assumption of an unknown cosmic ray composition above 10^{17} eV. The model and mass dependence of the invisible energy carried by neutrinos and energetic muons is calculated for the QGSjet [12] and SIBYLL [13, 14] models of hadronic interactions. The mean position of the shower maximum, $X_{\max}$, and its distribution is discussed as a measure of the primary cosmic ray composition and proton-air cross section in Sec. III. A summary and conclusions are given in Sec. IV.

II. SHOWER TRACK LENGTH AND ENERGY RECONSTRUCTION

Using the particle number as primary observable, an accurate Monte Carlo calculation of the electromagnetic energy in a shower requires that all the contributions to the track length due to electrons and positrons are properly accounted for. This implies computing the track length of electrons of a very wide energy range, including very small energies, since electrons with kinetic energy below 0.1 MeV typically account for $\sim 10\%$ of the electromagnetic energy [4]. A part of the energy of the primary particle is not converted to electromagnetic particles and hence not deposited as ionization energy in the atmosphere. High-energy muons deposit only a small fraction of their energy in the atmosphere and neutrinos escape detection completely. Therefore experiments have to correct for the "unseen" energy to estimate the primary particle energy. In a Monte Carlo simulation, once $E_{\rm em}$ is determined, the "unseen" energy can be calculated on a shower-by-shower basis as the difference to the primary particle energy.

In this section we calculate the fraction of shower energy that is not detected by a fluorescence experiment and we study its dependence on shower energy, on the primary nucleus that initiates the shower, and on the hadronic interaction model needed to extrapolate to unmeasured regions of the phase space of the primary nucleus-air collision. We compare the resolution achieved with two different estimators of shower energy, namely the track length integral and the number of particles at shower maximum. For this purpose we simulate large samples of showers and extract their longitudinal profile.

We use a fast hybrid simulation program [15] that allows the simulation of longitudinal shower profiles of electrons and muons. The hybrid method consists of calculating shower observables by a direct simulation of the initial part of the shower, tracking all particles of energy above $E_{\rm thr} = 0.01\ E$. Parameterizations of presimulated showers for all subthreshold particles are then superimposed after their first interaction point is sampled. The sub-showers are described with parameterizations that give the correct average behavior, and at the same time describe the fluctuations in shower development of both electrons and muons.

Electromagnetic cascades are simulated with a full-screening electromagnetic Monte Carlo at high energy and at low energy the longitudinal development of electromagnetic sub-showers is calculated using Greisen's parameterization [16]. The numerical approximation as given in [17] is applied with electron-induced showers being shifted by 0.8 radiation lengths [18]. Greisen's formula is a good approximation to the numerical solution of the cascade equations with vanishing low-energy cutoff.

In order to apply Eq. (1) to estimate shower energy from the number of particles given by our hybrid approach, the factor $\alpha_{\rm eff}$ in Eq. (1) must be determined for our approximation of electromagnetic showers. We normalize the track length predicted by our hybrid method to the electromagnetic energy in photon initiated showers of energy $E_{\rm em}$, turning photoproduction interactions artificially off to avoid that a fraction of $E_{\rm em}$ goes into a muonic and neutrino component,

$$\alpha_{\rm eff} = \frac{E_{\rm em}}{\int N(X) dX} \ . \qquad (2)$$

We obtain the numerical value $\alpha_{\rm eff} = 2.32$ MeV/g cm^{-2}, which we will use throughout this paper. It is important to realize that $\alpha_{\rm eff}$ depends on the treatment of low energy particles due to the different kinetic energy thresholds of the Monte Carlo simulations, and therefore our result cannot be directly compared to the numerical value obtained by Song et al. ($\alpha_{\rm eff} = 2.19$ MeV/g cm^{-2}) [4] who performed a CORSIKA [19] simulation with the threshold of 100 keV. Song et al. estimated that about 10% of the electromagnetic energy is carried by particles of kinetic energy less than 100 keV, which are neither included in the track length simulation nor in the calculation of $\alpha_{\rm eff}$. The value of 2.42 MeV/g cm^{-2} found by Risse and Heck (Fig. 7 in [11]) is not in contradiction with our result as it refers to a simulation threshold of 250 keV. In contrast to [4] the analysis in [11] defines $\alpha_{\rm eff}$ as the proportionality constant between the projected track length of all particles above simulation threshold and the total calorimetric energy, including the expected energy deposit of the particles falling below the simulation threshold.

A. Unseen energy in hadron-induced atmospheric showers

We turn now to the study of the unseen energy in nucleus-induced showers. Using the hybrid method we have simulated showers initiated by protons, helium, carbon and iron at zenith angle $\theta = 45°$, down to the approximate observation level of the HiRes and Auger experiments corresponding to a vertical depth of $X_{\rm v} =$

870 g/cm^2. We have performed the simulations using two hadronic interaction models SIBYLL 2.1 [20] and QGSjet01 [12], with the aim to study the influence of the model predictions on the amount of unseen energy in the shower.

We calculate the total track length by performing the integral in depth of the longitudinal profile generated by the hybrid method. Similar to the method applied by air-fluorescence experiments the simulated curve is fit by the Gaisser-Hillas function [21]

$$N_{\rm GH}(X) = N_{\rm max} \left(\frac{X - X_0}{X_{\rm max} - X_0}\right)^{(X_{\rm max}-X_0)/\lambda} \times \exp\left[-\frac{(X - X_{\rm max})}{\lambda}\right], \quad (3)$$

where X_0 is the depth of the first interaction, $X_{\rm max}$ is the depth at which the number of electrons in the shower is maximal, and $N_{\rm max}$ is the number of electrons at maximum. First the position of the shower maximum and the particle number at maximum are found by a polynomial fit to the shower profile near its maximum. In a subsequent fit the parameters λ and X_0 are determined. The unseen energy $E_{\rm u}$ in a shower of energy E then follows from

$$E_{\rm u} = E - E_{\rm em} = E - \alpha_{\rm eff} \int_0^\infty N_{\rm GH}(X) dX \ . \quad (4)$$

In figure 1 we plot the mean unseen energy as obtained in showers initiated by different nuclei and compare the predictions of the interaction models SIBYLL 2.1 and QGSjet01. The energy that is transferred to muons and neutrinos decreases with shower energy for all nuclei in both models. The main reason for this behavior is that as shower energy increases the average energy of charged pions increases as well, and in turn their probability of decaying into muons and neutrinos diminishes. At fixed energy the unseen energy is larger in showers initiated by heavy nuclei than in those induced by light nuclei. This can be understood on the basis of the superposition model in which a shower induced by a nucleus of A nucleons and energy E is considered as A independent proton showers of energy E/A, in each of which the fraction of unseen energy is larger than in a proton shower of energy E (Fig. 1). In fact, the muon number in a proton shower scales as $N_\mu \sim E^\alpha$ with $\alpha = 0.86 \ldots 0.92$ [15], and applying the superposition model it can be easily seen that an iron shower has about 1.5 times more muons than a proton shower of the same energy.

The unseen energy reaches almost a constant value at shower energy above $10^{19} - 10^{20}$ eV, and is fairly insensitive to composition in this energy region, the relative difference between the unseen energy fractions among the different nuclei being $\sim 10\%$. Interestingly the difference between the two model predictions is much bigger and essentially stays the same. At ultra-high energy the uncertainty in the missing energy assignment is dominated by the model dependence and not by an unknown primary composition.

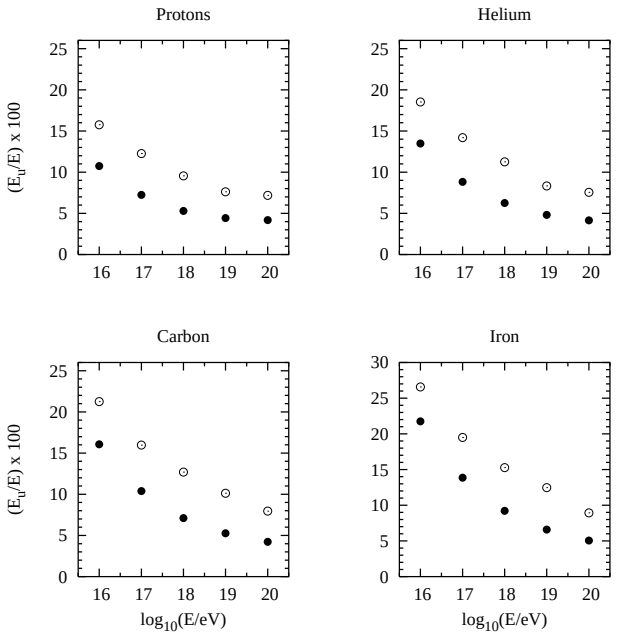

FIG. 1: Fraction of the total shower energy that is not seen by a fluorescence detector in showers initiated by proton, helium, carbon and iron as a function of shower energy E. 5,000 showers at zenith angle $\theta = 45^\circ$ were simulated for each hadronic interaction model: SIBYLL 2.1 (bold circles) and QGSjet01 (open circles).

The unseen energy predicted by QGSjet01 is consistently larger than the corresponding energy predicted by SIBYLL 2.1, the reason being that the muon multiplicity ($E_\mu > 0.3$ GeV) in QGSjet01 is larger than in SIBYLL 2.1. For example, QGSjet predicts about 35% more muons than SIBYLL 2.1 in proton-induced showers at 10^{20} eV [15]. This difference arises mainly due to the different multiplicities of secondaries predicted by the two models. The relative difference between the saturation values of the unseen energy predicted by SIBYLL and QGSjet is $\sim 50\%$. This translates to a 5% uncertainty for the total energy estimate.

Our results for the unseen energy fraction are similar to those obtained in [4] and recently in [22]. For example, Song et al. find a fraction of unseen energy of about 7% (10%) at $E = 10^{20}$ eV for proton (iron) showers and QGSjet98 [4]. Barbosa et al. have also used SIBYLL 2.1 in their simulations. They obtain an unseen energy fraction of about 5% and 8% for proton and iron showers at 10^{20} eV simulated with the SIBYLL model [22]. There are differences of the order of 1-3% between these calculations and our results which we attribute to the different low-energy interaction models used for the simulations, the approximative character of Greisen's parametrization for low-energy electromagnetic sub-showers, and different methods of calculating the track length integral. The latter involves extrapolating the electromagnetic shower component to larger atmospheric depths.

B. Shower energy reconstruction from the longitudinal shower profile

There are several methods to reconstruct the primary energy of an observed air shower profile experimentally. Not only the total shower track length in the atmosphere in Eq. (1) but also the number of particles at shower maximum can serve as an estimator of the shower energy. The latter one is of particular interest for nearly vertical showers where only the first part of the shower can be observed and the uncertainty in the calculation of the total track length could be dominated by the extrapolation of the shower profile into the unobserved region. In this section we study the energy resolution that is achieved with these two methods.

As previously discussed, shower energy can be calculated from the measured track length. The procedure is to fit a Gaisser-Hillas or other function to the observed longitudinal profile [23], integrate it to obtain the total track length, extract the energy that goes into the electromagnetic component and correct it for the unseen energy that is estimated by Monte Carlo simulations.

The procedure above is subject to uncertainties because, usually, a previously calculated mean value of the missing energy, averaged over many simulated showers, is used to determine the energy of each individual event. Moreover, due to fluctuations in the shower longitudinal profile the experiments are unable to determine the type of primary nucleus that initiated the shower on an event-by-event basis. In consequence a correction for missing energy averaged over different primaries must be used. In addition the correction for unseen energy depends on the hadronic interaction model used to perform the simulations.

We estimate the energy of the shower (E_t) from the track length obtained as indicated above in the following way,

$$E_t = \langle f_u \rangle E_{\rm em} = \langle f_u \rangle \alpha_{\rm eff} \int_0^\infty N_{\rm GH}(X) dX \qquad (5)$$

where $\langle f_u \rangle$ is the average value of the correction for the energy not seen. The value of $\langle f_u \rangle$ depends on $E_{\rm em}$ and is for simplicity taken as the arithmetic mean over a uniform four-component mass composition, i.e. $\langle f_u \rangle = (\sum_i f_u^i)/4$ where $f_u^i = E_{\rm em}/E$ are the corrections for unseen energy in showers initiated by different primary nuclei. The index i corresponds to proton, helium, carbon and iron induced showers. For fixed primary particle type, f_u^i was obtained as the average value of $E_{\rm em}/E$ in 5,000 simulated showers.

Alternatively, shower energy can also be estimated from the size of the electron distribution at shower maximum $N_{\rm max}$. The relation between $N_{\rm max}$ and energy can be expressed as $E = gN_{\rm max}$ where g must be obtained by Monte Carlo simulations. As before, the determination of shower energy is subject to uncertainties because g has to be averaged over many showers and different primaries, and is also model dependent. Then the estimated energy of a shower (E_N) follows from $N_{\rm max}$ through the equation,

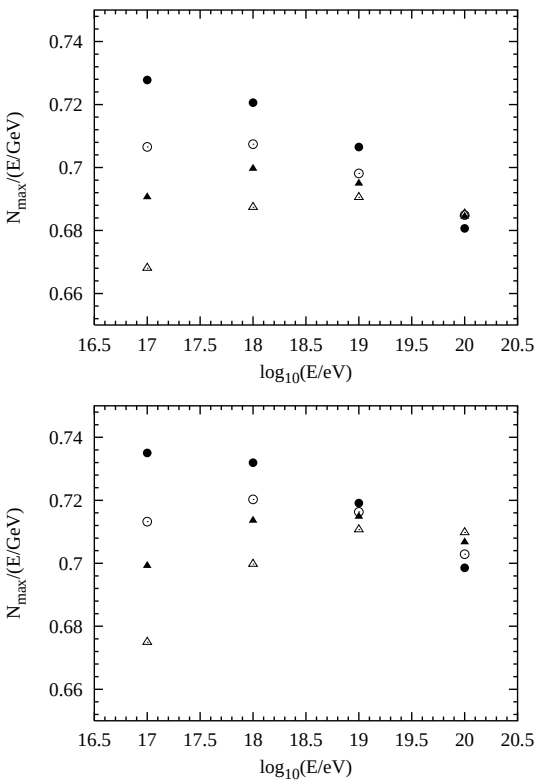

FIG. 2: Average shower size at maximum normalized to shower energy in GeV in showers initiated by proton (bold circles), helium (open circles), carbon (bold triangles) and iron (open triangles) as a function of shower energy E. 5,000 showers at zenith angle $\theta = 45^\circ$ were simulated for each hadronic interaction model: SIBYLL 2.1 (bottom panel) and QGSjet01 (top panel).

$$E_N = \langle g \rangle N_{\rm max} \ , \qquad (6)$$

where $\langle g \rangle = (\sum_i g_i)/4$ and the index i corresponds again to protons, helium, carbon and iron. The g_i values were obtained as the average of $E/N_{\rm max}$ in 5,000 simulated showers fixing the type of primary particle.

Figure 2 shows the average shower size at maximum as a function of energy in showers initiated by different nuclei. Each point represents an average over 5,000 showers. The results of SIBYLL 2.1 and QGSjet01 are presented. It is interesting to see how the dependence of $N_{\rm max}$ on composition changes with shower energy. In the energy region of 10^{19} to 10^{20} eV the value of $N_{\rm max}$ is rather composition-independent, making it a good energy estimator. However, the mass dependence is of the order of 10% in the energy range between 10^{17} and 10^{18} eV. The hadronic interaction model dependence for fixed energy and type of primary is remarkably small $\sim 1-2\%$.

For an experiment measuring showers with a steep energy spectrum the knowledge of the event-by-event correlation, i.e. the energy resolution, is of great importance.

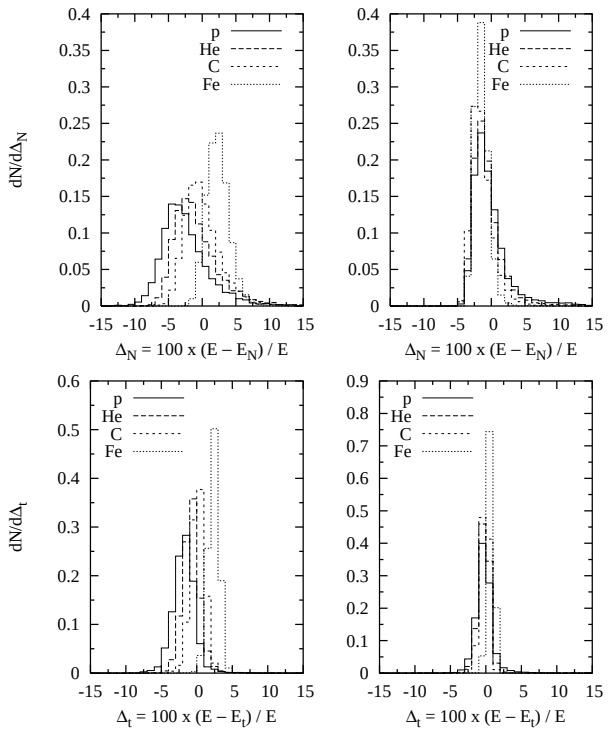

FIG. 3: Distributions of the error in shower energy determination for two energy estimators. The results are shown for different nuclei and for SIBYLL 2.1. Left panels $E = 10^{18}$ eV, right panels $E = 10^{20}$ eV. Top panels: $N_{\rm max}$ is used as energy estimator. Bottom panels: the energy estimator is the track length integral.

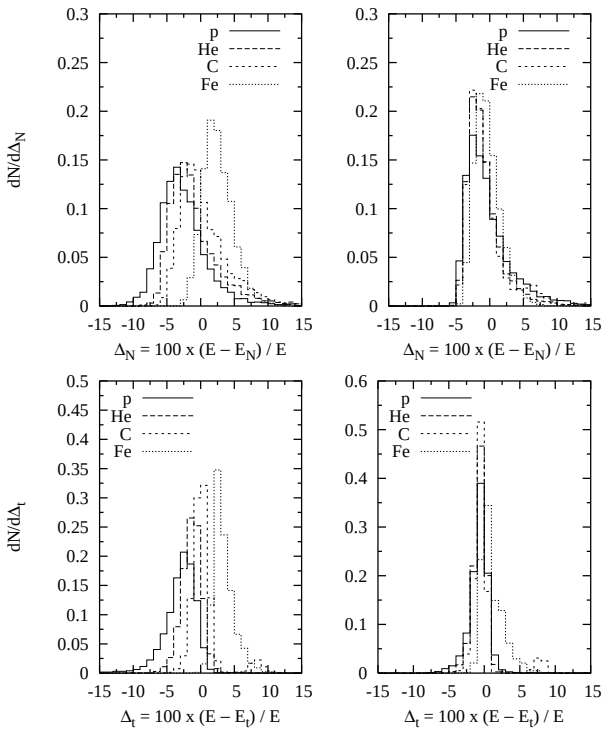

FIG. 4: Distributions of the error in shower energy determination for two energy estimators. The results are shown for different nuclei and for QGSjet01. Left panels $E = 10^{18}$ eV, right panels $E = 10^{20}$ eV. Top panels: $N_{\rm max}$ is used as energy estimator in the top panels. Bottom panels: the energy estimator is the track length integral.

In Fig. 3 we show the resolution in energy achieved with E_t in Eq. (5), and E_N in Eq. (6), for SIBYLL 2.1 at two representative shower energies. We plot the relative difference in percentage between the estimated energy (E_t or E_N) and the actual shower energy. Fig. 4 shows the corresponding energy resolution for QGSjet01. The mean values and standard deviations of the proton and iron distributions shown in Figs. 3 and 4 are given in tables I and II.

At energies above 10^{19} eV, the energy resolution achieved with $N_{\rm max}$ is similar to the one obtained when the track length is used as energy estimator. However the error in E with $N_{\rm max}$ is more asymmetric than the corresponding one for the track length, due to the intrinsic asymmetry of the distribution of $N_{\rm max}$ at $E = 10^{19} - 10^{20}$ eV (see for instance Fig. 11 in reference [15]). The asymmetry is less pronounced in the case of heavy nuclei.

Both energy estimators produce an energy resolution which is not strongly dependent on composition above $E = 10^{19}$ eV. This can be easily understood from Figs. 1 and 2 in which it can be seen that at $E > 10^{19}$ eV both the fraction of unseen energy in the shower and $N_{\rm max}$ are weakly dependent on the type of primary nucleus. The dependence on composition is more pronounced in the energy range $10^{17} - 10^{18}$ eV, on average a $\sim 5 - 7\%$ uncertainty in the energy determination with both methods is introduced if the nature of the primary is unknown. It is interesting to notice that both methods tend to underestimate the energy for proton primaries and overestimate it for iron primaries due to the assumption of a uniform four-component composition in all the energy range above 10^{17} eV. The systematic uncertainty introduced by the hadronic interaction model when using $N_{\rm max}$ as estimator is about 1%, comparable to the one in the case of the track length integral method.

In summary, $N_{\rm max}$ is a remarkably good energy estimator that may replace the total track length at energies above 10^{19} eV if care is taken for the asymmetric errors in the distributions. An $N_{\rm max}$-based energy determination may be superior to the track length method when only a small portion of the shower around the maximum is detected, for instance due to the limited sensitivity or acceptance of the fluorescence detector.

TABLE I: Mean value and standard deviation of the distributions of the error corresponding to the histograms for protons in Figs. 3 and 4.

Model	SIBYLL 2.1				QGSjet01			
$\log_{10}$(E/eV)	$\langle\Delta_t\rangle$	$\sigma(\Delta_t)$	$\langle\Delta_N\rangle$	$\sigma(\Delta_N)$	$\langle\Delta_t\rangle$	$\sigma(\Delta_t)$	$\langle\Delta_N\rangle$	$\sigma(\Delta_N)$
17.0	−3.2	6.1	−4.4	5.4	−3.8	6.8	−4.6	5.1
18.0	−1.8	2.6	−2.4	3.8	−3.0	6.7	−2.5	3.8
19.0	−0.9	1.7	−0.3	3.0	−2.3	2.0	−1.6	3.1
20.0	−0.2	2.0	−0.1	3.2	−0.8	2.2	−0.1	3.8

TABLE II: Mean value and standard deviation of the distributions of the error corresponding to the histograms for iron in Figs. 3 and 4.

Model	SIBYLL 2.1				QGSjet01			
$\log_{10}$(E/eV)	$\langle\Delta_t\rangle$	$\sigma(\Delta_t)$	$\langle\Delta_N\rangle$	$\sigma(\Delta_N)$	$\langle\Delta_t\rangle$	$\sigma(\Delta_t)$	$\langle\Delta_N\rangle$	$\sigma(\Delta_N)$
17.0	4.1	1.6	4.3	2.2	4.1	2.3	4.3	2.5
18.0	2.4	0.7	2.3	1.7	3.4	2.5	2.6	2.2
19.0	1.4	0.3	1.1	1.4	3.1	3.2	1.0	2.2
20.0	0.6	0.2	−1.4	1.1	1.1	2.7	−0.3	2.0

III. SHOWER LONGITUDINAL DEVELOPMENT AND P-AIR CROSS SECTION DETERMINATION

The most obvious, experiment-independent observable characterizing the longitudinal shower profile is the depth of maximum, $X_{\rm max}$. The mean depth of maximum is a good measure of the composition in units of the mean logarithmic mass. Indeed, within the superposition model one expects for a primary particle with mass number A

$$\langle X_{\rm max}^{(A)}\rangle = D_e \ln(E/A) = \langle X_{\rm max}^{(p)}\rangle - D_e \ln A, \qquad (7)$$

with D_e being the elongation rate, a weakly energy dependent parameter. The elongation rate reflects features of high-energy hadron production, see for example [15, 24], making the interpretation of measurements model-dependent. However not only the mean depth of maximum carries important information about both the primary cosmic ray composition and the features of the hadronic interactions, but also its distribution. A number of analyses using $X_{\rm max}$ distributions to infer the primary cosmic ray chemical composition are available in literature, for example [25, 26, 27]. In the following we will concentrate on the $X_{\rm max}$ distribution of showers in respect to the possibility and limitations of determining the features of the hadronic interactions, in particular of measuring the high-energy proton-air inelastic cross section.

The correlation of the first interaction point with the depth of shower maximum for proton showers was first employed by the Fly's Eye Collaboration in [28]. An analysis in the context of a mixed primary composition was done in [25], using the Fly's Eye data and more recently in [29] using HiRes data.

The probability of having the first interaction point of a shower, $X_{\rm int}$, at a depth greater than X is

$$P(X_{\rm int} > X) \propto \exp(-X/\lambda_{\rm int}), \qquad (8)$$

with the interaction length $\lambda_{\rm int} = \langle m\rangle/\sigma$. Here $\langle m\rangle$ is the mean mass of the air nuclei and σ denotes the inelastic, particle production cross section. In case of a perfect correlation between $X_{\rm max}$ and $X_{\rm int}$, i.e. in case fluctuations in shower development were non-existent, one could use directly the exponential distribution of showers with large $X_{\rm max}$ to calculate $X_{\rm int}$ and hence the proton-air cross section. However, intrinsic shower fluctuations modify the relation between the depth of maximum distribution and the interaction length. This modification is typically expressed by a factor k with

$$P(X_{\rm max} > X) = B\exp(-X/\Lambda), \quad \Lambda = k\lambda_{\rm int}\ . \qquad (9)$$

The factor k depends mainly on the pace of energy dissipation in the early stages of shower evolution. Concerning the models QGSjet and SIBYLL we have the interesting situation that, if one considers the mean depth of maximum, $\langle X_{\rm max}\rangle$, the mean inelasticity compensates to some extent the differences in the cross sections. For example, SIBYLL predicts the larger proton-air cross section but at the same time a smaller inelasticity than QGSjet. In contrast, the ratio $\Lambda/\lambda_{\rm int}$, i.e. the k factor, is sensitive to the inelasticity fluctuations. In general, a model with small fluctuations in secondary particle multiplicity and inelasticity is characterized by a smaller k factor than a model with large fluctuations. Under the

assumption of similar fluctuations in multiplicity and inelasticity, a model predicting a large average number of secondary particles leads to smaller overall fluctuations of the cumulative shower profile of the secondary particles and hence to a smaller k factor. Therefore the parameter Λ is very sensitive to the hadronic interaction model and its measurement would allow one to draw conclusions on general features of high-energy hadron production [30]. Conversely, knowing the k factor for a given model one can measure the proton-air cross section.

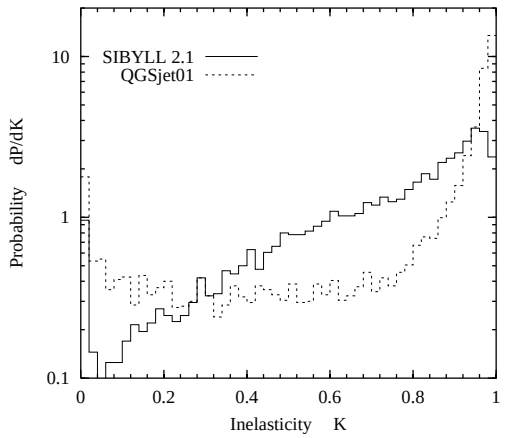

FIG. 5: Inelasticity distribution in p-air collisions at $E = 10^{19}$eV.

In Fig. 5 we show the inelasticity distribution in proton-air interactions at 10^{19}eV simulated with SIBYLL 2.1 and QGSjet01. Here inelasticity K is defined as $K = (E - E_{\rm lead})/E$ with $E_{\rm lead}$ being the energy of the fastest baryon (p, n, or Λ) and E the projectile energy. Although the mean inelasticities predicted by QGSjet and SIBYLL are similar (0.77 and 0.72 respectively), the pronounced peaks at small and large inelasticities in QGSjet events induce somewhat larger shower-to-shower fluctuations (see below). The large difference in the predicted mean charged particle multiplicities (QGSjet: 540, SIBYLL: 315 at $E = 10^{19}$ eV [15]) is of lesser importance since most of the secondary particles are very slow.

Fig. 6 shows the $X_{\rm max}$ distributions for proton showers at fixed energies as predicted by QGSjet01 and SIBYLL 2.1. The different slopes of the tails of the distributions stem from the different slopes of the exponential first interaction probability (Eq. (8)), and the different intrinsic shower fluctuations predicted by the models. In table III we give the numerical values of the slope of the $X_{\rm max}$ distribution, Λ, obtained by doing an exponential fit to the tail of the SIBYLL and QGSjet distributions using Eq. (9).

In the absence of internal fluctuations, all showers would develop through the same amount of matter, ΔX, between the first interaction point and maximum. As a consequence, a perfect correlation between $X_{\rm max}$ and $X_{\rm int}$ would exist, and their distributions would have exactly the same shape, shifted by a constant $\Delta X = X_{\rm max} - X_{\rm int}$. In that case the slope of the $X_{\rm max}$ distribution Λ would be equal to the mean interaction length $\lambda_{\rm int}$. Table III compares the predictions of SIBYLL 2.1 and QGSjet01 on these three quantities. Also shown in the table is the standard deviation of the distribution in ΔX, which gives an idea of the size of the fluctuations in the shower longitudinal profile.

The effect of fluctuations in ΔX is to broaden the correlation of $X_{\rm max}$ with $X_{\rm int}$ and to change its slope. SIBYLL 2.1 predicts less fluctuations than QGSjet01, the difference between the widths of the ΔX distributions is however fairly small $\sim\ 6 - 7$ g/cm^2. The different fluctuations of the two models are also reflected in the larger width of the QGSjet01 $X_{\rm max}$ distribution compared to SIBYLL 2.1. QGSjet01 also predicts a smaller p-air cross section (larger $\lambda_{\rm int}$) than SIBYLL 2.1. This, added to the fact that the intrinsic fluctuations in shower development are larger in QGSjet01, makes the slope of the QGSjet distribution in $X_{\rm max}$ flatter than the SIBYLL one, as can be seen in Fig. 6 and in table III. Interestingly, the k factors in SIBYLL and QGSjet01 are very similar within their statistical errors, somewhat larger in QGSjet01 (table III). This means that the difference in the slopes of the $X_{\rm max}$ distributions is dominated by the different p-air interaction lengths predicted by the models, implying that the larger intrinsic shower fluctuations of QGSjet01 play a less important role. This conclusion is different when the same analysis is done for the old version of QGSjet, namely QGSjet98. QGSjet98 predicts larger fluctuations than QGSjet01, mainly due to a larger diffractive cross section, added to the fact that both versions have the same total and inelastic cross section and hence the same p-air interaction length. The larger multiplicity predicted by QGSjet01 further reduces the fluctuations. As a consequence QGSjet98 predicts larger k-factors than QGSjet01 and SIBYLL 2.1. Numerical values of k in QGSjet98 for energies $E = 10^{18}, 10^{19}$ and 10^{20} eV are $k = 1.20 \pm 0.02,\ 1.24 \pm 0.02$ and 1.16 ± 0.02 respectively, the corresponding reduced χ^2 are $\chi^2/{\rm dof} = 0.56,\ 0.91$ and 1.18 [31].

Finally, within a single model (QGSjet01 or SIBYLL 2.1), the k-factors depend very weakly on primary energy. This is just reflecting the weak energy dependence of the intrinsic shower fluctuations as can be demonstrated by looking at the values of $\sigma(\Delta X)$ in table III.

A. Influence of fitting range on k-factor determination

There are a number of complications making the measurement of the parameter Λ difficult. First, the $X_{\rm max}$ distribution is not a perfect single exponential. As a consequence the k-factor depends on which part of the $X_{\rm max}$ distribution is used for fitting. This is illustrated in Fig. 7 where a non-constant k factor as a function of the smallest $X_{\rm max}$ considered in the fit ($X_{\rm max}^{\rm cut}$), is shown for SIBYLL and QGSjet respectively. To test how well a single exponential would describe the tail of

TABLE III: p-air interaction length ($\lambda_{\rm int}$), slope of the fitted tail of the $X_{\rm max}$ distribution (Λ), and standard deviation of the $X_{\rm max}$ and $\Delta X = X_{\rm max} - X_{\rm int}$ distributions (all in g/cm^2), where $X_{\rm max}$ is the depth of shower maximum, and $X_{\rm int}$ is the depth at which the first p-air interaction occurs. These quantities are shown for different shower energies as predicted by SIBYLL 2.1 and QGSjet01. 30,000 proton showers were simulated to make each of the distributions. The fit to the tail of the $X_{\rm max}$ distribution in order to obtain the numerical values of Λ and $k = \Lambda/\lambda_{\rm int}$ was performed using only the trailing edge of the distribution, 100 g/cm^2 beyond the peak of the distribution i.e., $X_{\rm max} > X_{\rm max}^{\rm peak} + 100$ g/cm^2. Also shown is the χ^2/dof of the fit. Errors, where shown, are statistical.

Model	SIBYLL 2.1						QGSjet01					
E [eV]	$\lambda_{\rm int}$	Λ	$\sigma(X_{\rm max})$	$\sigma(\Delta X)$	k	χ^2/dof	$\lambda_{\rm int}$	Λ	$\sigma(X_{\rm max})$	$\sigma(\Delta X)$	k	χ^2/dof
10^{18}	43.64	50.63 ± 0.70	59.03	39.16	1.15 ± 0.03	1.24	48.44	58.33 ± 0.87	66.34	44.94	1.18 ± 0.03	1.83
10^{19}	39.49	47.12 ± 0.68	54.74	37.66	1.16 ± 0.02	1.08	44.93	53.58 ± 0.85	63.32	44.79	1.18 ± 0.02	0.90
10^{20}	35.93	42.49 ± 0.73	51.18	37.56	1.14 ± 0.03	0.94	41.89	49.28 ± 0.69	59.98	44.51	1.14 ± 0.02	0.79

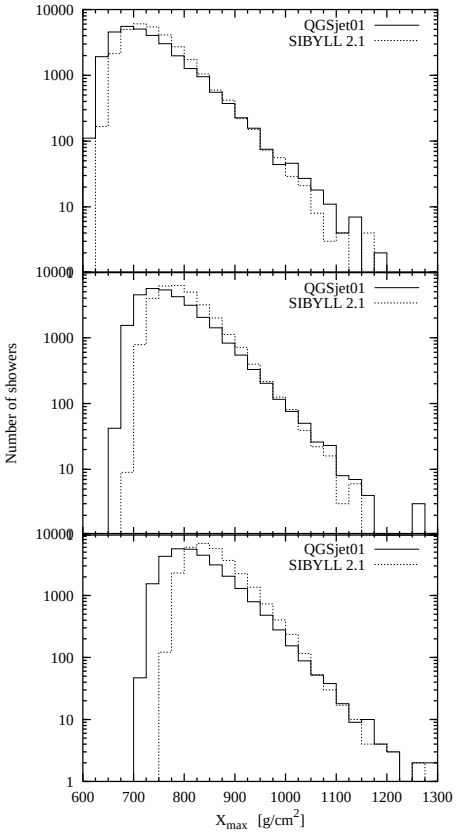

FIG. 6: Distribution of the depth of maximum of proton-induced showers at energies $E = 10^{18}$, 10^{19} and 10^{20} eV (from top to bottom panels). 30,000 showers were simulated with QGSjet01 (solid histogram) and SIBYLL2.1 (dotted histogram).

the $X_{\rm max}$ distributions in both models, we made fits of the k factor as function of $X_{\rm max}^{\rm cut}$, assuming k being constant. The mean values are $k = 1.15 \pm 0.01,\ 1.16 \pm 0.01$ and 1.16 ± 0.01 at $E = 10^{18},\ 10^{19}$ and 10^{20} eV respectively for SIBYLL 2.1, the corresponding χ^2 values per degree of freedom being χ^2/dof $= 0.25,\ 0.71$ and 1.6. For QGSjet01 the corresponding values of k and χ^2/dof are: $k = 1.18 \pm 0.01,\ 1.18 \pm 0.01,\ 1.16 \pm 0.01$ and $\chi^2 = 0.65,\ 0.60,\ 1.48$.

The hypothesis of a flat behavior of k versus $X_{\rm max}^{\rm cut}$ is not as bad as Fig. 7 might indicate. The large errors of the points at large $X_{\rm max}^{\rm cut}$, although they deviate most from a constant value, have the smallest weights in the fit and do not affect much χ^2/dof. The large errors stem from the lack of statistics in the far tail of the $X_{\rm max}$ distribution [32]. These errors might introduce large uncertainties in the determination of the p-air inelastic cross section, especially if a cut at large $X_{\rm max}$ has to be applied in order to avoid contamination by other nuclear species that might be present in the primary cosmic ray spectrum. This last issue is the subject of subsection C below.

B. Influence of resolution in $X_{\rm max}$ on k-factor determination

So far we have assumed an ideal experiment which is able to measure the depth of maximum with infinite resolution i.e., $\Delta X_{\rm max} = 0$. However in the real world the accuracy is not infinite, in fact the HiRes collaboration has published a value of $\Delta X_{\rm max} \sim 35$ g/cm^2 for the resolution in the depth of maximum [27, 29]. The purpose of this subsection is to explore the effect of the finite resolution on the numerical value of the k factor. For this purpose we take the $X_{\rm max}$ distribution obtained before assuming a perfect resolution, and we smear it with a Gaussian of standard deviation equal to the $X_{\rm max}$ resolution reported by HiRes. An example of the effect of this smearing on the original distribution is shown in Fig. 8. As expected the smeared distribution is wider than the original one (by about 15 g/cm^2). However the slope of the distribution is not significantly modified, and as a consequence the change in the k factor is still within its estimated statistical error. This is demonstrated in table IV where the k factors obtained from the non-smeared

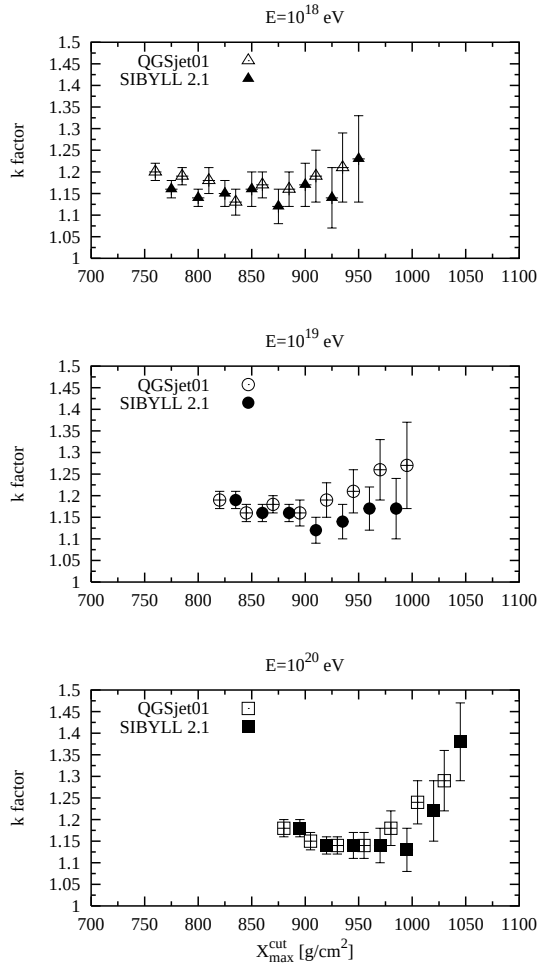

FIG. 7: Numerical values of the k factor for proton-initiated showers simulated with SIBYLL 2.1 (full symbols) and QGSjet01 (empty symbols) in dependence on the considered minimal atmospheric depth, $X_{\rm max}^{\rm cut}$, above which the fit to the tail of the distribution in $X_{\rm max}$ is performed. 30,000 showers were simulated to make the distributions.

and the smeared distributions are presented for SIBYLL and QGSjet.

C. Influence of composition on k-factor determination

A second complication in the determination of the inelastic p-air cross section arises due to the mass composition of the primary cosmic rays. Contamination of the proton spectrum by heavier elements may lead to changes in the measured parameter Λ and hence a misinterpretation of the data in terms of the cross section or k factor. To investigate this issue we simulated iron showers and contaminated the proton spectrum assuming the primary cosmic ray composition reported by the HiRes collaboration consisting on 70% protons and 30%

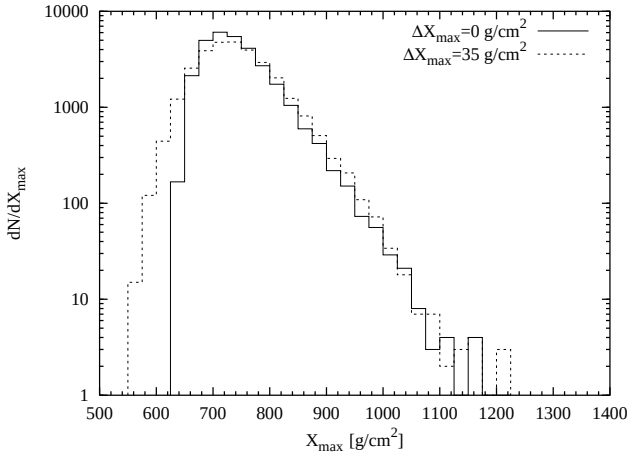

FIG. 8: Distribution of the depth of maximum of proton-induced showers at energy $E = 10^{18}$ eV. 30,000 showers were simulated with SIBYLL2.1. The solid histogram is the non-smeared, perfect $X_{\rm max}$ resolution distribution, and the dashed histogram is the solid distribution after smearing it with a Gaussian of standard deviation $\Delta X_{\rm max} = 35$ g/cm^2.

iron [27]. We assumed that the composition is energy-independent in the energy range between 10^{18} eV and 10^{20} eV, as indicated by the HiRes data [27].

Figs. 9, 10 show the distributions of $X_{\rm max}$ for the measured HiRes composition, as predicted by the models SIBYLL 2.1 and QGSjet01 respectively. A Gaussian $X_{\rm max}$ resolution of standard deviation $\Delta X_{\rm max} = 35$ g/cm^2 was folded in both the proton and the iron distributions. The figures also show the individual contributions. As is clearly seen, a fraction of 30% of iron nuclei does not significantly contribute to the total distribution beyond the peak. In fact the change of slope with respect to a pure protonic composition is very small, almost negligible in the tail of the distribution 100 g/cm^2 beyond the peaks of the distributions. This conclusion applies for both SIBYLL and QGSjet. As a consequence the k factors do not change with respect to those given in table IV for protons with a resolution in $X_{\rm max}$ of 35 g/cm^2.

Clearly if helium, being the nuclear species that produces the largest average $X_{\rm max}$, is present in the cosmic ray spectrum in this energy range, the contamination might be more important and a cut well beyond the peak of the distribution, in the far tail of the total distribution, has to be performed in order to avoid a bias in the cross section determination. The exact position of the cut depends on the fraction of helium in the primary cosmic ray spectrum. To further investigate this point we also simulated helium-induced showers at $E = 10^{18}$ eV and we plot the distribution in $X_{\rm max}$ for a composition with varying fractions of protons and helium and a constant fraction of 30% iron. This is shown in Fig. 11. The k-factors obtained when fitting the three $X_{\rm max}$ distributions in fig. 11 using only the region 100 g/cm^2 beyond its peak, are: $k = 1.19 \pm 0.02$, 1.15 ± 0.02 and 1.07 ± 0.02 for fractions of proton+helium $70\% + 0\%$, $50\% + 20\%$

TABLE IV: Standard deviation of the $\Delta X = X_{\max} - X_{\rm int}$ distribution, k factors and reduced χ^2 of the fits performed in order to obtain k. These quantities are shown for a non-smeared perfect $X_{\max}$ resolution distribution, and for the same distribution after smearing it with a Gaussian error $\Delta X_{\max} = 35$ g/cm^2. The results of SIBYLL 2.1 and QGSjet01 hadronic interaction models are shown. Errors, where shown, are statistical. Only the trailing edge of the distribution 100 g/cm^2 beyond shower maximum is used to make the fits.

Model	SIBYLL 2.1				QGSjet01			
$\Delta X_{\max}$	0 g/cm^2		35 g/cm^2		0 g/cm^2		35 g/cm^2	
E [eV]	k	χ^2/dof	k	χ^2/dof	k	χ^2/dof	k	χ^2/dof
10^{18}	1.15 ± 0.03	1.24	1.18 ± 0.03	1.80	1.18 ± 0.03	1.83	1.19 ± 0.02	0.76
10^{19}	1.16 ± 0.02	1.08	1.18 ± 0.02	1.06	1.18 ± 0.02	0.90	1.17 ± 0.02	0.75
10^{20}	1.14 ± 0.03	0.94	1.20 ± 0.03	1.62	1.14 ± 0.02	0.79	1.15 ± 0.02	0.50

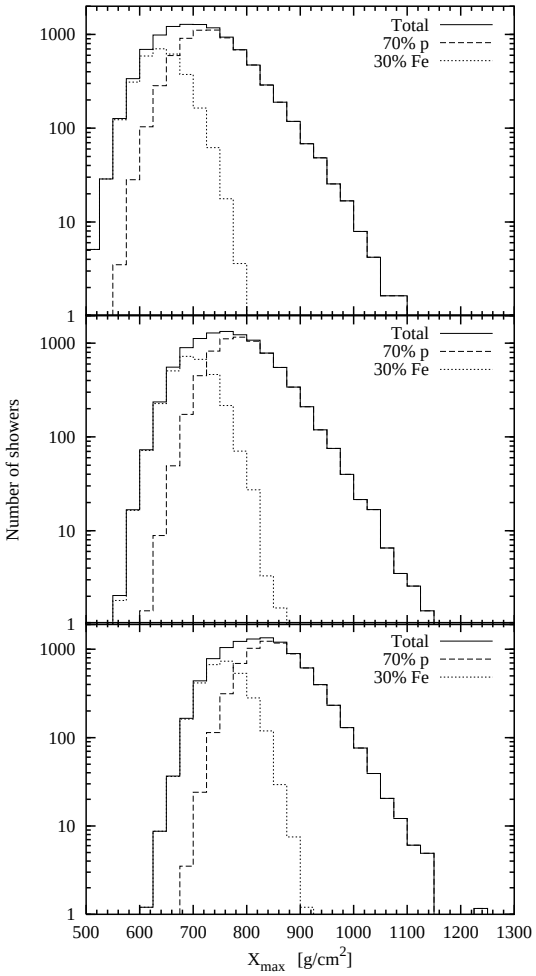

FIG. 9: Depth of maximum distributions for a composition consistent on 70% protons and 30% iron nuclei. From top to bottom panels the primary energy is $E = 10^{18}$, 10^{19} and 10^{20} eV. The distributions were obtained using the SIBYLL 2.1 hadronic generator. A $X_{\max}$ Gaussian resolution of 35 g/cm^2 was folded in.

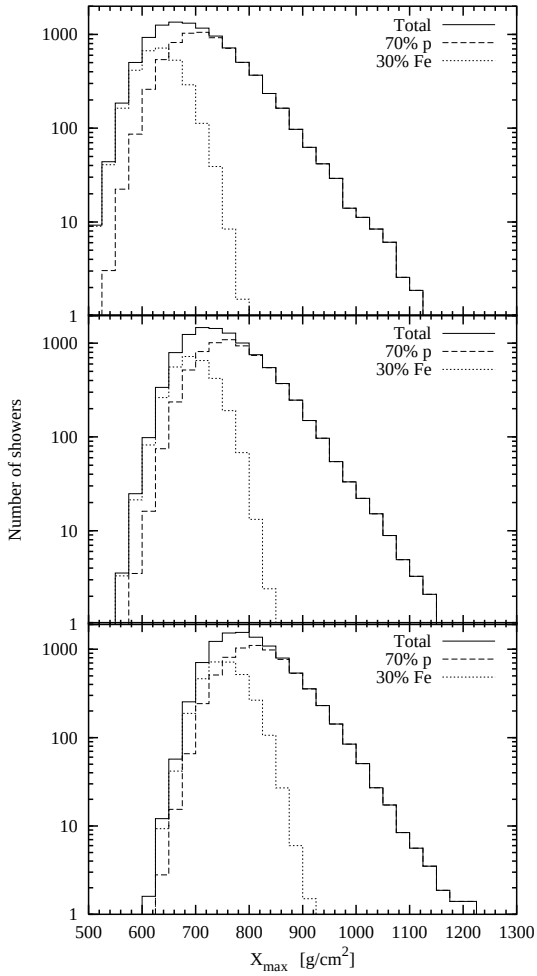

FIG. 10: Same as Fig. 9 for QGSjet01.

and $30\% + 40\%$ respectively, keeping the fraction of iron constant. Clearly, if no cut is applied at $X_{\max}$ larger than the nominal value of 100 g/cm^2 beyond the peak of the distribution, an important systematic bias is introduced.

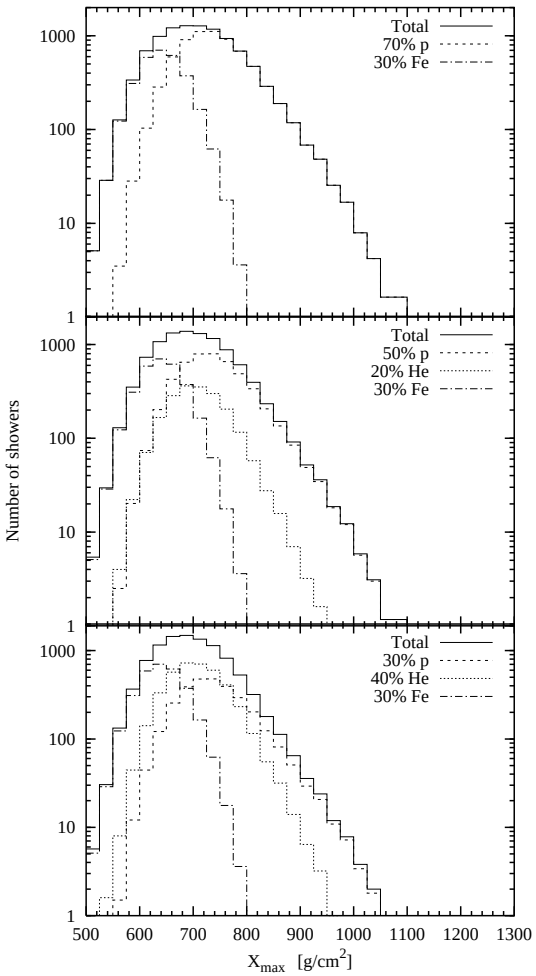

FIG. 11: Depth of maximum distributions for a composition consisting of 70% protons and 30% iron nuclei (top panel), 50% protons, 20% helium and 30% iron nuclei (middle panel), and 30% protons, 40% helium and 30% iron nuclei (bottom panel). The primary energy is $E = 10^{18}$. The distributions were obtained using the SIBYLL 2.1 hadronic generator. A $X_{\rm max}$ Gaussian resolution of 35 g/cm^2 was folded in.

This will induce an error in the determination of the cross section if there is a relatively large ($> 20\%$) fraction of helium nuclei in the primary cosmic ray spectrum.

IV. SUMMARY AND CONCLUSIONS

We have used a hybrid simulation scheme [15] for a quantitative evaluation of certain systematic uncertainties in the interpretation of fluorescence measurements of giant air showers. The sources of uncertainty we investigate include the model of hadronic interactions used for shower simulation, the unknown mixture of primary nuclei in the cosmic radiation and intrinsic fluctuations in shower development. We do not investigate uncertainties in shower reconstruction, detector acceptance or other technical aspects related to properties of the environment or performance of the detectors.

As an illustration of uncertainties arising from the need to extrapolate hadronic interaction models outside the kinematical region and energies explored by accelerator experiments, we compared two specific interaction models, QGSjet [12] and SIBYLL [13], both of which agree with each other and with a range of accelerator data for $\sqrt{s} \sim$ TeV and below. We find that the correction for unseen energy (i.e. energy lost to neutrinos and muons that reach the ground) is consistently larger for QGSjet than for SIBYLL. The difference is such that, for a given track length integral, the assigned energy will be about 5% higher when the same data are interpreted with QGSjet rather than with SIBYLL.

For primary energies below about 10^{19} eV/nucleus the fraction of unseen energy depends significantly on the mass of the primary nucleus. For example, at 10^{17} eV with SIBYLL about 7% of the primary energy is lost to neutrinos and muons as compared to 13% for iron.

In view of the steep cosmic-ray energy spectrum, knowledge of the energy resolution is of great importance. The track length integral can be used to assign energy when a sufficient portion of the profile is measured to fix the parameters needed to complete the integral. It has an intrinsic resolution of 2-4%, depending somewhat on interaction model and energy (narrower at higher energy). Size of shower at maximum gives only a marginally broader energy resolution (3-5%) and can be used when much of the profile after maximum is not measured, provided care is taken to correct for a slightly asymmetric distribution. There is in both methods some dependence on primary mass of the relation between the measured quantity and the primary energy which leads to a $\sim 5\%$ systematic uncertainty if the primary mass is not separately determined.

Intrinsic fluctuations in shower development (after the first interaction) affect the relation between the interaction length ($\lambda_{\rm int}$) and the slope Λ that describes the exponential tail of the $X_{\rm max}$ distribution. The relation is often expressed with a 'k factor as $\Lambda = k \times \lambda_{\rm int}$. Differences in k factors for the range of models studied here are at the level of 5-7%, implying a similar uncertainty in the p-air cross section that may be inferred from measurements of shower profiles. Further uncertainties arise to the extent that an unknown fraction of helium and other nuclei contaminate the tail of the measured $X_{\rm max}$ distribution.

Acknowledgments J.A. Ortiz is supported by CNPq/Brasil and acknowledges the Bartol Research Institute for its hospitality. This research is supported in part by NASA Grant NAG5-10919. RE, TKG & TS are also supported by the US Department of Energy contract DE-FG02 91ER 40626. JA-M is also supported by MCyT (FPA 2001-3837 and FPA 2002-01161). The simulations presented here were performed on Beowulf clusters funded by NSF grant ATM-9977692.

[1] R. M. Baltrusaitis et al., Nucl. Instrum. Meth. **A264**, 87 (1988).

[2] T. Abu-Zayyad et al., Nucl. Instrum. Meth. **A450**, 253 (2000).

[3] J. Cronin et al., The Pierre Auger Project design report 2$^{\rm nd}$ ed. Available at Auger website www.auger.org (1995).

[4] C. Song et al., Astropart. Phys. **14**, 7 (2000).

[5] R. M. Baltrusaitis et al., Nucl. Instrum. Meth. **A240**, 410 (1985).

[6] M. Risse and D. Heck (2003), astro-ph/0308158, to appear in Astropart. Phys.

[7] F. Kakimoto et al., Nucl. Instrum. Meth. **A372**, 527 (1996).

[8] M. Nagano, K. Kobayakawa, N. Sakaki, and K. Ando, Astropart. Phys. **20**, 293 (2003), astro-ph/0303193.

[9] B. Dawson (2002), Auger GAP note GAP-2002-067, available at www.auger.org.

[10] J. Alvarez-Muñiz et al., Phys. Rev. **D67**, 101303 (2003).

[11] M. Risse and D. Heck (2002), Auger GAP note GAP-2002-043, available at www.auger.org.

[12] N. N. Kalmykov, S. S. Ostapchenko, and A. I. Pavlov, Nucl. Phys. B (Proc. Suppl.) **52B**, 17 (1997).

[13] R. Engel, T. K. Gaisser, P. Lipari, and T. Stanev (2000), in *Proceedings of the 26th Int Cosmic Ray Conference*, Salt Lake City, Utah, USA, 1999, (AIP, Melville, NY, 2000), Vol. 1, p. 415.

[14] R. S. Fletcher, T. K. Gaisser, P. Lipari, and T. Stanev, Phys. Rev. D **50**, 5710 (1994).

[15] J. Alvarez-Muñiz, R. Engel, T. K. Gaisser, J. A. Ortiz, and T. Stanev, Phys. Rev. **D66**, 033011 (2002).

[16] B. Rossi and K. Greisen, Rev. Mod. Phys. **13**, 240 (1941).

[17] K. Greisen, Prog. Cosmic Ray Physics **3**, 1 (1956).

[18] T. K. Gaisser, P. Lipari, and T. Stanev (1997), in *Proceedings of the 25th International Cosmic Ray Conference*, Durban, South Africa, 1997, (World Scientific, Singapore, 1997), Vol. 6, p. 281.

[19] D. Heck, J. Knapp, J. Capdevielle, G. Schatz, and T. Thouw (1998), wissenschaftliche Berichte, Forschungszentrum Karlsruhe.

[20] R. Engel, T. K. Gaisser, and T. Stanev (2001), in *Proceedings of the 27th International Cosmic Ray Conference*, Hamburg, Germany, 2001, (Copernicus Gesellschaft, Katlemburg-Lindau, 2001), p. 431.

[21] T. K. Gaisser, *Cosmic Rays and Particle Physics* (Cambridge University Press, Cambridge, 1990).

[22] H. M. J. Barbosa, F. Catalani, J. A. Chinellato, and C. Dobrigkeit (2003), astro-ph/0310234.

[23] T. Abu-Zayyad et al. (HIRES), Astropart. Phys. **16**, 1 (2001).

[24] J. Linsley and A. A. Watson, Phys. Rev. Lett. **46**, 459 (1981).

[25] T. K. Gaisser et al., Phys. Rev. **D47**, 1919 (1993).

[26] T. Abu-Zayyad et al. (HiRes-MIA), Astrophys. J. **557**, 686 (2001), astro-ph/0010652.

[27] G. Archbold et al. (2003), in *Proceedings of the 28th International Cosmic Ray Conference*, Tsukuba, Japan, 2003, (Universal Academy Press, Inc., Tokyo, Japan, 2003), p. 405.

[28] R. M. Baltrusaitis et al., Phys. Rev. Lett. **52**, 1380 (1984).

[29] K. Belov et al. (2003), in *Proceedings of the 28th International Cosmic Ray Conference*, Tsukuba, Japan, 2003, (Universal Academy Press, Inc., Tokyo, Japan, 2003), p. 1567.

[30] M. M. Block, F. Halzen, and T. Stanev, Phys. Rev. Lett. **83**, 4926 (1999), hep-ph/9908222.

[31] The fit to the tail of the $X_{\rm max}$ distribution in order to obtain the numerical values of k was performed using only the trailing edge of the distribution 100 g/cm^2 beyond its peak.

[32] Despite the fact that we have simulated 30,000 showers.